Segmentation of Bone Structures in 3D CT Images Based on Continuous Max-flow Optimization

J. A. Pérez-Carrasco[a], B. Acha[a] and C. Serrano[a]

[a]University of Seville Signal and Communications Dpt. Camino de los Descubrimientos, s/n. 41092,Seville,Spain

ABSTRACT

In this paper an algorithm to carry out the automatic segmentation of bone structures in 3D CT images has been implemented. Automatic segmentation of bone structures is of special interest for radiologists and surgeons to analyze bone diseases or to plan some surgical interventions. This task is very complicated as bones usually present intensities overlapping with those of surrounding tissues. This overlapping is mainly due to the composition of bones and to the presence of some diseases such as Osteoarthritis, Osteoporosis, etc. Moreover, segmentation of bone structures is a very time-consuming task due to the 3D essence of the bones. Usually, this segmentation is implemented manually or with algorithms using simple techniques such as thresholding and thus providing bad results. In this paper gray information and 3D statistical information have been combined to be used as input to a continuous max-flow algorithm. Twenty CT images have been tested and different coefficients have been computed to assess the performance of our implementation. Dice and Sensitivity values above 0.91 and 0.97 respectively were obtained. A comparison with Level Sets and thresholding techniques has been carried out and our results outperformed them in terms of accuracy.

Keywords: Segmentation, CT, Max-flow, Optimization

1. INTRODUCTION

Automatic and accurate segmentation of bones is of special interest for radiologists and surgeons in order to analyze and locate many kinds of fractures, to diagnose some bone diseases (such as Osteoarthritis, Rheumatoid Arthritis, Osteoporosis) and in plastic surgical planning. The segmentation of such structures is difficult because the presence of some diseases usually provokes a reduction in bone density in different areas. Besides, the different parts of the bones (mainly periosteum, compact (hard) bone, cancellous (spongy) bone and bone marrow) present wide differences in densities and thus, different Hounsfield values.[1] This implies an overlapping of these values with other tissue types such as muscle, fat or some organs.

In Fig. 1 several bone structures can be seen. It can be seen in the figure that the presence of a wide range of different Hounsfield values in these structures make the segmentation problem more coplicated (note the different Hounsfiel values in cortical and cancellous bone).

A second difficulty in the segmentation of bone structures is their 3D essence. Thus, fast and automatic algorithms are required in order to obtain the segmentation with reduced computational times.

Many algorithms have been published regarding to bone segmentation and, according to Wang et al.,[2] they can be classified into four categories: intensity-based,[3] edge-based,[4] region-based,[5] and model-based.[4,6] In some works the segmentation technique is selected according to the number of bones or type of bone to be segmented.[7–9] This lack of generalization is a problem, as radiologists do not want to consider different segmentation methods according to the regions to be analyzed. Thus, a more general method more suitable for a wide number of bone structures would be desirable. When considering more general methods, level sets, active contours and graph cuts implementations are preferred.[10–12] However, level set methods can drive to

Further author information: (Send correspondence to J. A. Pérez-Carrasco)
J. A. Pérez-Carrasco: E-mail: jperez2@us.es, Telephone: +34 954 48 73 33
B. Acha: E-mail: bacha@us.es, Telephone: +34 954 48 73 33
C. Serrano: E-mail: cserrano@us.es, Telephone: +34 954 48 73 33

Medical Imaging 2015: Image Processing, edited by Sébastien Ourselin, Martin A. Styner, Proc. of SPIE Vol. 9413, 94133Y · © 2015 SPIE · CCC code: 1605-7422/15/$18 · doi: 10.1117/12.2082139

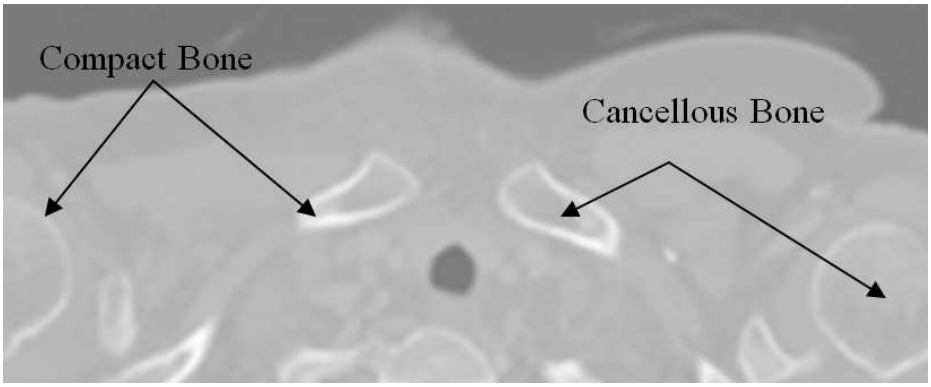

Figure 1. Zoomed abdominal section of a CT volume. Note differences in compact bone with cancellous bone in the different bone structures.

local optima of the minimization energy function and suffer from high sensitivity to initialization. Graph cut techniques have the advantage that they guarantee the global optima (if bipartition is implemented and a Potts model is adopted) in nearly real time.

In the algorithm presented in this paper, a methodology based on continuous convex relaxation techniques[13,14] is followed. We combine gray level information, gradient values and statistical information computed using histogram distances and provide this combined information as input to a convex relaxation algorithm in order to get accurate and fast segmentation of bones in 3D volumes. Continuous convex relaxation techniques share the advantages of both active curves and graph-cuts[14] and they outperform graph cuts in regard to speed and accuracy.[14]

2. METHOD

The methodology implemented in the work presented in this paper consists in three steps. The first step is a bone enhancement operation. Hounsfield values in CT volumes are usually between -2000 and 3000. The bones usually have values from 700 (cancellous bone) to 3000 (dense bone) approximately. In order to get a higher contrast, a thresholding operation followed by a normalization operation has been applied to the different images used throughout our experiments. The resulting normalized image is denoted as *Inorm*. The threshold, maximum and minimum values used during the two operations are common in all the volumes that have been used in order to not lose generalization.

The second stage of our algorithm is the computation of Histogram Distance Images (HDI). 10% of the volumes used throughout our experiments have been used to obtain a model histogram of bone structures. The rest 90% of the volumes were used to test our algorithm and for comparison purposes. In this dataset, for each voxel (i, j, k), a local histogram is computed. Different 3D sizes of this local neighborhood were tested and a local neighborhood of 7x7x3 provided the best results. Subsequently, for each local histogram, a distance[17] to the histogram model is calculated and this distance is assigned to voxel (i, j, k) in a new Histogram Distance Image (HDI). HDI will have values close to 0 in regions where bone tissue appears and close to 1 when no bones are encountered. Finally, in order to combine this 3D statistic information with the gray level information *Inorm*, we create a cost image term to be minimized (CIT) as:

$$CIT = ((1 - Inorm) + HDI)/2 \tag{1}$$

Eq. 1 is the cost to be minimized using the continuous max-flow algorithm described in the next subsection. The first term of the right expression in Eq. 1 uses intensity information. Pixels corresponding to bone (mainly cortical bone) will have values close to '1'. Thus, we use $1 - Inorm$ instead of *Inorm* directly because we want low values in bone structures. Something similar occurs with the second term in the right expression in Eq. 1. The distance to the model histogram in pixels corresponding to bones should be close to 0 whereas it should be close to 1 in pixels belonging to other kind of tissues. In Fig. 2 these computed images are shown for a CT

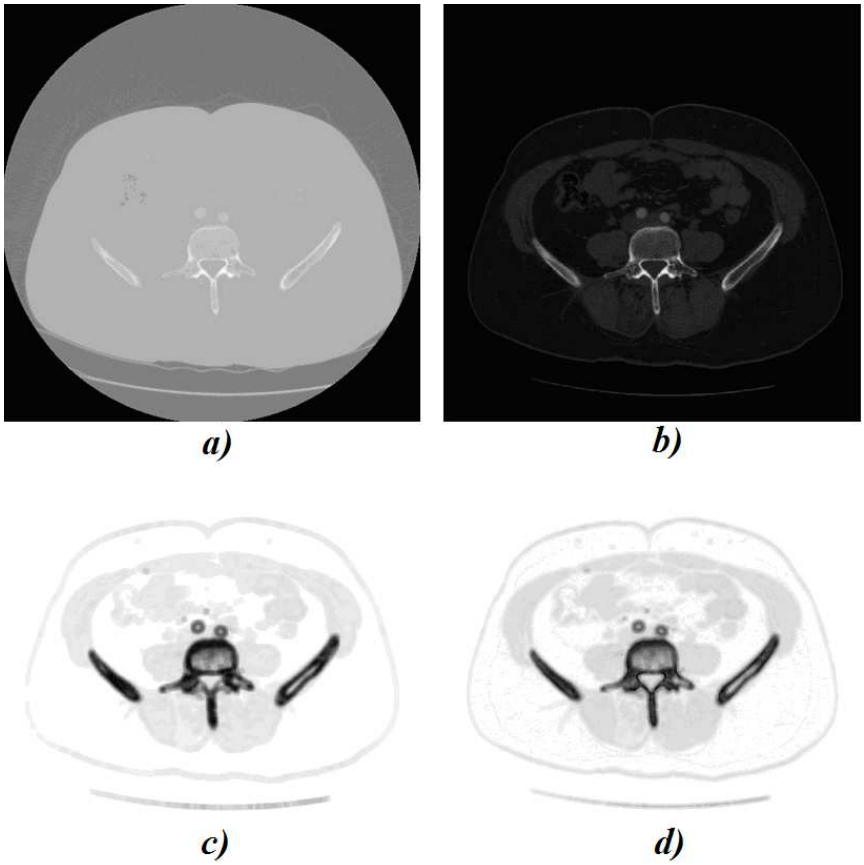

Figure 2. Computed images used by the algorithm. The first image (a) is the initial image without thresholding. The second image (b) corresponds to the thresholded and normalized image. The third image (c) corresponds to the distance image *HDI*. Finally, the last image (d) shows the new computed image *CIT*.

slice. The first image (a) is the initial image without thresholding. The second image (b) corresponds to the thresholded and normalized image. The third image (c) corresponds to the distance image *HDI*. Finally, the last image (d) corresponds to *CIT* image which will be the input to the continuous max-flow algorithm. It can be seen that bone structures are darker in *CIT* image, which means that gray level information and distance between histograms information have been properly combined.

Finally, in the last and third stage, we use the *CIT* image above computed, as input to the continuous max-flow optimization algorithm proposed by J. Yuan et al.[13] In the work by Yuan et al., citeYuan20102217, Yuan et al. proved that the max-flow problem, which is formulated by maximizing the total flow from the source, is equivalent to a continuous s-t min-cut problem as follows:

$$\min_{u(x)\epsilon[0,1]} \int_{\Omega} (u)C_s dx + \int_{\Omega} (1-u)C_t dx + \int_{\Omega} C(x)|\nabla u| dx \tag{2}$$

u(x) is the labeling function and indicates if point x belongs to the region to be segmented. If the minimization problem is well defined, the cost function C_s should take low values inside the bones and high values outside them. Similarly, C_t should take low values outside the bones and high values inside them. The most right term of Eq. (2) is the regularization term and $C(x)$ is a penalty function. $|\nabla u|$ is the absolute gradient of the labeling function $u(x)$, thus indicating the boundary of the segmented region. C_s and C_t are called regional terms. In the algorithm proposed here, the regional term C_s, provided as input to the continuous max-flow algorithm, is

the CIT image computed through Eq. (1). Thus, in the algorithm proposed, the terms C_s and C_t (Eq. 2) are computed as follows:

$$C_s = CIT \tag{3}$$

$$C_t = 1 - CIT \tag{4}$$

Note that with Eq. (4) we force C_t to be low outside the bones and high inside them, as required by the minimization in (2). In addition, the algorithm penalizes an excessive area of the surface limiting the segmented volume. This penalization term is the most right term in Eq. (2). This penalization is modeled by a function $C(x)$ depending on the gradient of the CIT image along the surface, so that if the gradient is high along the surface, a large area of the surface is not penalized. The penalization function is computed as follows:

$$C(x) = \frac{b}{1 + a|\nabla CIT(x)|} \tag{5}$$

where parameters a and b control the importance of the gradient in the penalization function. In our implementation a and b values have been obtained empirically and their values are 10 and 0.2, respectively. Note that at the surface, $|\nabla u|$ will have high values whereas $C(x)$ will have low values if the gradient of $CIT(x)$ is high. Thus, the most right term in Eq. 2 will not penalize a large area if a high border is encountered.

Finally, in order to smooth out the resulting segmented image, and to get a more accurate segmentation, a morphological operation of opening is performed.

It is important to note that the proposed algorithm uses the gradient information that is very high in the boundaries of cortical bone structures and histogram distance information, which is very useful mainly to segment cancellous bone structures, which present lower gray values and overlap with other tissue types such as muscle, fat or some organs.

3. EXPERIMENTAL RESULTS

To assess the algorithm proposed, twenty images corresponding to ten different patients have been used. Manual segmentations of all the slices were provided by an expert. Three different methods have been compared using the same set of images. Table 1 shows the performance parameters provided by each of the techniques. These parameters are the *Jaccard*, *Dice*, Sensitivity (S) and Positive Predictive Value (PPV) parameters. Both *Jaccard* and *DICE* coefficients measure the set agreement in terms of false positive, false negative, true negative and true positive counts.

Table 1. Comparison between the three different algorithms.

METHOD	Computational Time	PPV	Sensitivity	Specificity	Dice	Jaccard
THRESHOLDING	0,017 s	0,8	0,802	0,993	0,7857	0,656
DRLSE	3402 s	0,54	0,938	0,889	0,6031	0,511
thresholded HDI	**255 s**	**0.872**	**0.9570**	**0.9946**	**0.9106**	**0.8397**

The first method was a technique based on thresholding. A common threshold was computed for all the images and the threshold providing the best results was 1200. As it has been stated before, the low results provided by this method are because bone structures do not have a pixel-wise constant object distribution, which means that they are composed by different structures with different Hounsfield values.

The second method employed has been the Distance Regularized Level Set Evolution (*DRLSE*) published in Ref. 18. In the experiments shown in Ref. 18, low computational times were obtained when small images with a reduced number of regions were employed. However, when bigger images are considered and many different bone structures are considered, performance values were considerably low and excessively high computational times were required. In all these cases the algorithm used to have convergence problems. Table 1 shows the results when using $Inorm$ image as input and using parameters $\lambda = 20$, timestep $\Delta t = 5$, $\epsilon = 1.5$ and $\alpha = 1$.

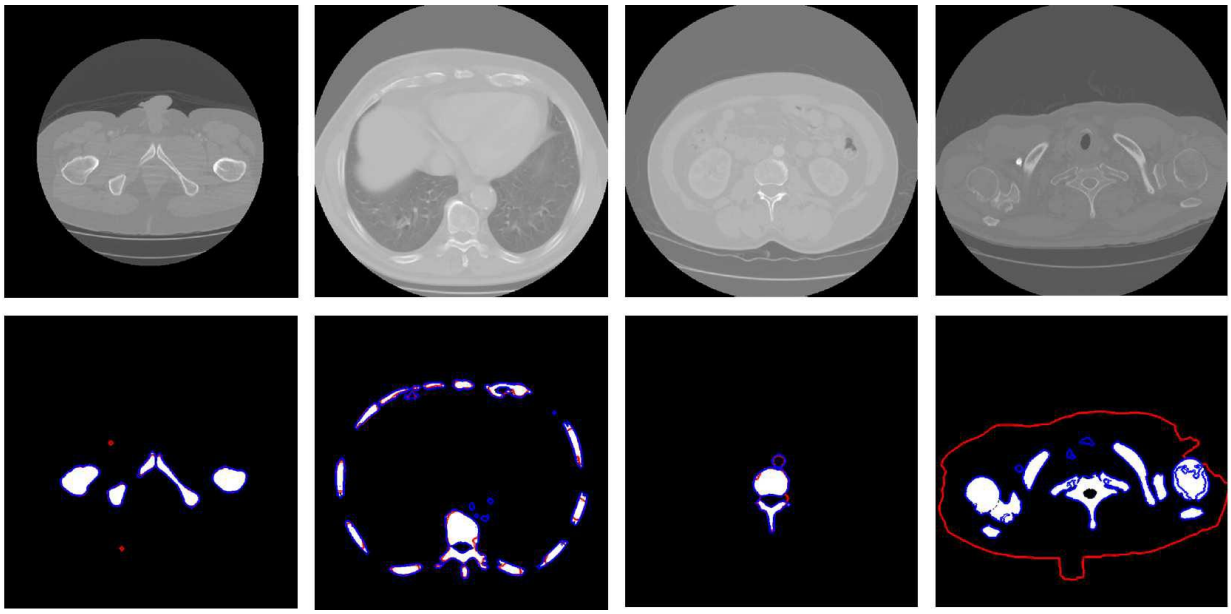

Figure 3. Results obtained for four different images using our algorithm. Upper row shows the original images. Lower row shows the corresponding groundtruth images. Results obtained with the *DRLSE* algorithm are shown in red. Results provided by our algorithm are shown in blue.

The third method corresponds to our algorithm and it has been labeled as thresholded *HDI*. Only pixels above a threshold value were considered to compute the *HDI* image. Using this thresholding operation a reduction of 80% in the computational time was obtained when compared with the same technique without thresholding.

Fig. 3 shows the results obtained for four different images using our algorithm and *DRLSE*. Note how the *DRLSE* algorithm has problems when some bone structures have inner regions that do not correspond to bones.

The segmentation step corresponding to the continuous max-flow algorithm offered an average computational cost of $0.5s$ per $512x512$ slice, which is much smaller than values provided by other minimization strategies. The creation of the HDI image was the most time consuming task (see Table 1). Matlab 7.12 was used in all the experiments.

4. CONCLUSIONS

The segmentation of bone structures is a complicated task because they present intensities overlapping with those of surrounding tissues. In this paper an automatic algorithm, which combines gray level information and statistical information extracted from local histograms in a 3D neighborhood of the voxels under consideration, is computed for segmentation of bone structures. The gray information and the statistical information are combined and used as input to a continuous max-flow optimization algorithm. Several coefficients have been computed to measure the algorithm performance. Results obtained are over 0.9, which indicates neither the FP rate nor the FN rate are high. High sensitivity values above 0.97 were obtained. A further validation, with a higher number cases would be desirable. Note that the segmentation stage using a continuous max-flow implementation is faster than the majority of algorithms in the literature. Future implementations will speed up the creation of the input image *CIT*, which is the main bottleneck in our implementation.

The authors declare that the work is not being, or not has been, submitted for publication or presentation elsewhere.

ACKNOWLEDGMENTS

This research has been supported by TEC2010-21619-C04-02 and P11-TIC-7727.

REFERENCES

[1] Feeman, T. G., [*The mathematics of medical imaging: A beginner's guide*], Springer undergraduate texts in mathematics and technology. Springer (2010).

[2] Wang, L. G., et al., "Validation of bone segmentation and improved 3-D registration using contour coherency in CT data," *IEEE Transactions on Medical Imaging*, 25(3), 324–334, (2006).

[3] Kang, Y., et al., "A new accurate and precise 3-D segmentation method for skeletal structures in volumetric CT data," *IEEE Transactions on Medical Imaging*, 22(5), 586–598, (2003).

[4] Pardo, X. M., et al., "A snake for CT image segmentation integrating region and edge information," *Image and Vision Computing*, 19(7), 461–475, (2001).

[5] Beveridge, J. R., et al., "Segmenting images using localized histograms and region merging," *International Journal of Computer Vision*, 2(3), 311–347, (1989).

[6] Sebastian, T. B., et al., "Segmentation of carpal bones from CT images using skeletally coupled deformable models," *Medical Image Analysis*, 7(1), 2–45, (2003).

[7] Cheng, Y., et al., "Automatic segmentation technique for acetabulum and femoral head in CT images," *Pattern Recognition*, 46(11), 2969–2984, (2013).

[8] Cervinka, T., Hyttinen, J., Sievnen, H., "Accurate cortical bone detection in peripheral quantitative computed tomography images," *in IFMBE Proceedings*, 289–292, (2014).

[9] Aslan, M. S., et al., "A novel 3D segmentation of vertebral bones from volumetric CT images using graph cuts," *Lecture Notes in Computer Science*, **5876** LNCS, 519–528, (2009).

[10] Shadid, W., Willis, A., "Bone fragment segmentation from 3D CT imagery using the Probabilistic Watershed Transform," *in Conference Proceedings - IEEE SOUTHEASTCON*, (2013).

[11] Calder, J., et al., "A variational approach to bone segmentation in CT images," *in Progress in Biomedical Optics and Imaging*, SPIE (2011).

[12] Kratky, J., "Three-dimensional segmentation of bones from CT and MRI using fast level sets," *in Progress in Biomedical Optics and Imaging*, SPIE, (2008).

[13] Yuan, J., Bae, E., Tai, X. C., "A study on continuous max-flow and min-cut approaches," *in Proceedings of CVPR*, 2217–2224, (2010).

[14] Punithakumar, K., Yuan, J., "A Convex Max-Flow Approach to Distribution-Based Figure-Ground Separation," *SIAM Journal of Imaging Sciences*, 5(4),1333–1354, (2012).

[15] Chan, T. F., et al., "Algorithms for finding global minimizers of image segmentation and denoising models," *SIAM Journal on Applied Mathematics*, 66(5), 1632–648, (2006).

[16] Bresson, X., et al., "Fast global minimization of the active contour/snake model," *Journal of Mathematical Imaging and Vision*, 28(2), 151–167, (2007).

[17] Rubner, Y., et al., "The Earth Mover's Distance as a Metric for Image Retrieval," *International Journal of Computer Vision*, 40(2), 99–121, (2000).

[18] Li, C., Xu, C., Gui, C., Fox, M. D., "Distance Regularized Level Set Evolution and its Application to Image Segmentation," *IEEE Trans. Image Processing*, 19(12), 3243–3254, (2010).